

Article

Preferable Adsorption of Nitrogen and Phosphorus from Agricultural Wastewater Using Thermally Modified Zeolite–Diatomite Composite Adsorbent

Boyang Zhang¹, Xiaoling Wang^{2,*}, Songmin Li^{3,*}, Yuyang Liu¹, Yucheng An¹ and Xiaotong Zheng¹

¹ School of Environmental Science and Engineering, Tianjin University, Tianjin 300072, China; zhangby@tju.edu.cn (B.Z.); 15122267857@163.com (Y.L.); anyuchentju@163.com (Y.A.); zhengxiaotong@tju.edu.cn (X.Z.)

² State Key Laboratory of Hydraulic Engineering Simulation and Safety, Tianjin University, Tianjin 300072, China

³ Department of Water Conservancy Engineering, Tianjin Agriculture University, Tianjin 300384, China

* Correspondence: wangxl@tju.edu.cn (X.W.); lisongmin228@126.com (S.L.); Tel.: +86-022-2789-0911 (X.W.)

Received: 21 July 2019; Accepted: 29 September 2019; Published: 30 September 2019



Abstract: Nitrogen and phosphorus adsorbents are widely used to mitigate agricultural non-point source pollution. However, research on adsorbents mainly involves studying chemical adsorption properties, and analyzes of the effects of adsorbent on pollutant removal has not considered the surface morphology of the adsorbent or the surface distribution of pollutants. In this study, we focus on the surface morphology of the adsorbent and the surface distribution of contaminants while examining chemical adsorption properties. The crystal composition of the adsorbent was evaluated by x-ray diffraction (XRD) characterization. Kinetic adsorption data and adsorption isotherms demonstrated that thermally modified zeolite exhibits better nitrogen adsorption. The optimal removal of nitrogen and phosphorus by thermally modified zeolite and diatomite occurred at a 3:2 ratio, reaching a removal rate of 92.07% and 84.61%, respectively. The potential adsorption mechanism of a composite adsorbent for nitrogen and phosphorus capture was investigated by Fourier transform infrared spectroscopy. Scanning electron microscopy mapping, grey image recognition, and gradient recognition confirmed a relationship between the surface morphology of the adsorbent and the distribution of surface pollutants. The larger the surface of the gradient, the more uneven it is, the more nitrogen and phosphorus sites are adsorbed on the surface, and the more nitrogen and phosphorus are adsorbed. These results suggest that thermally modified zeolite/diatomite can serve as a promising adsorbent for nitrogen and phosphorus removal in practical applications.

Keywords: composite adsorbent; thermally modified zeolite; diatomite; SEM mapping; grey image recognition; gradient recognition

1. Introduction

Presently, based on farmland drainage ditches, agricultural non-point pollution control technology has been focused on ecological ditches, and nitrogen and phosphorus adsorbent as a kind of adsorption material has had wide application in the treatment of agricultural non-point source pollution in rivers and lakes. Furthermore, nitrogen and phosphorus adsorbents have advantages in terms of stable performance, a wide range of application, efficiency, simple operation and artificial controllability [1]. The use of adsorbents with strong adsorption of nitrogen and phosphorus in farmland drainage ditches can improve the efficiency of the interception and absorption of nitrogen and phosphorus; therefore, these adsorbents can help considerably in controlling agricultural non-point source pollution.

At present, several adsorbents have been developed and utilised to remove pollutants from water, including acid soil, smectite, kaolinite, ceramicite, aluminium oxide, activated carbons, graphene oxide, and diatomite, as well as zeolite [2–4]. He et al. [5] proposed a composite adsorbent in which lanthanum oxide was incorporated onto porous zeolite (La-Z), preferably phosphate. Based on the adsorption kinetics, isotherms, pH, and interfering ion effect, porous zeolite-supported lanthanum oxide was shown to be an excellent material to adsorb phosphate. Wu et al. [6] proposed a novel granular adsorbent fabricated with zeolite and Al-Mn binary oxide to remove ammonium-nitrogen (NH_4^+ -N) and phosphorus (P) from contaminated water. Mahardika et al. [7] investigated granular activated carbon impregnated with amorphous ferrihydrite for adsorption of phosphorus from water solution and increased the uptake of phosphorus by preoxidation treatment. Goscianska et al. [8] proposed a new low-cost synthetic zeolite obtained from fly ash and modified with lanthanum to remove phosphate from aqueous solution. A number of adsorbents are used to remove nitrogen and phosphorus pollutants from water. Among them, the adsorption of ammonia by zeolite and phosphorus by diatomite has become a hot topic in current research. Therefore, this study conducted in-depth research on these two adsorbents.

There are also many studies on the adsorption mechanism. The improved adsorption capacity of three kinds of smectite for ammonia nitrogen was proposed based on clay characterization methods and adsorption experiments [9]. Pertaining to the influence of adsorption capacity, the effects of pH, background electrolyte cations and heavy metal were investigated, e.g., the effect of tetracycline adsorption onto kaolinite [10]. Fe_3O_4 /kaolin magnetic nanocomposites by the chemical co-precipitation method were proposed, and the effects of contact time, initial dye concentration, adsorbent dose, temperature, and initial pH of the solution on the adsorption process were studied [11]. The chemical adsorption mechanism was further analyzed by FT-IR, x-ray photoelectron spectroscopy (XPS), and UV-VIS is spectroscopy [12]. Skubiszewska-Ziba et al. [13] investigated a carbon-mineral adsorbent (CMA) prepared using complex diatomaceous earth/perlite adsorbent that was spent in the purification of apple juice and carbonised with the addition of starch or glucose to enhance the content of carbon deposits and develop the porosity of the CMA. In an effort to increase the effectiveness of removing ammonium ion from natural zeolite, Widiastuti et al. [14] examined the theoretical aspects of adsorption, including adsorption isotherms, kinetics, and thermodynamics, as well as desorption-regeneration studies. Li et al. [15] conducted a study on the preparation of β -cyclodextrin polymers. The adsorption behaviour of β -Cd polymer for Pb, Cu, and Cd was investigated in terms of adsorption kinetics, isotherms, and thermodynamics. Li et al. [16] modified starch nanoparticles and systematically investigated their stability and adsorption properties. Yang et al. [17] fabricated an adsorbent from N-doped porous carbon sheets resulting from wheat straws through the use of molten salts via the carbonisation-functionalisation process. Fang et al. [18] provided a new method to describe an adsorbent particle's surface element of pollutant distribution based on statistical results.

According to these studies, many different adsorbents have been proposed for particular pollutants. Ultimately, most of the studies concentrated on modifying the inner structure, which seems to be a key point of adsorbent research. Adsorbents have also been analyzed based on some conventional methods, such as the study of adsorption kinetics and isotherms. Some of the issues that remain are as follows: (1) how to break through the limit of conventional methods and go deeper into methods to characterize the adsorption process, (2) how to reflect the process of chemical adsorption more clearly and prepare high-efficiency adsorbents, and (3) how to use greyscale and gradient recognition to reveal the adsorption process.

Based on the above issues, the content of this study includes the following aspects: (1) A more intuitive method is proposed that can distinctly explain the adsorption process of nitrogen and phosphorus. In detail, the distribution of nitrogen and phosphorus on the surface was determined by adsorption images obtained by scanning electron microscopy (SEM) mapping and judging the surface configuration of the adsorbent by greyscale and gradient recognition of SEM images. (2) Adsorption properties were studied by kinetic and isothermal adsorption experiments, and the ratio of composite

adsorbents was determined based on equilibrium adsorption experiments with different ratios. (3) The adsorption mechanism, characterized by FT-IR and XRD analysis, was investigated to reveal changes in the functional groups and main material components in the adsorption process.

To achieve these targets, this paper is organized as follows: First, an analysis is presented based on the provided XRD data. XRD mainly observes the chemical composition inside an adsorbent. Then, the adsorption kinetics and isotherm experiments for natural zeolite, modified zeolite, and diatomite are performed in which an adsorbent is selected for high-efficiency removal of nitrogen and phosphorus and mixed into a composite adsorbent. Next, the optimal ratio of the composite adsorbent is determined by testing its adsorption properties. The composite adsorbent exhibiting the best adsorption performance is characterized by SEM, FT-IR, and SEM mapping. SEM is used mainly to observe the surface morphology of the adsorbent, FT-IR mainly measures the surface functional groups of the adsorbent, and SEM mapping characterization is mainly used to monitor the pollutant particles adsorbed on the surface of the adsorbent. Surface adsorption conditions were studied by using greyscale and surface gradient recognition, through which the surface configuration is evaluated, as shown in the research framework in Figure 1.

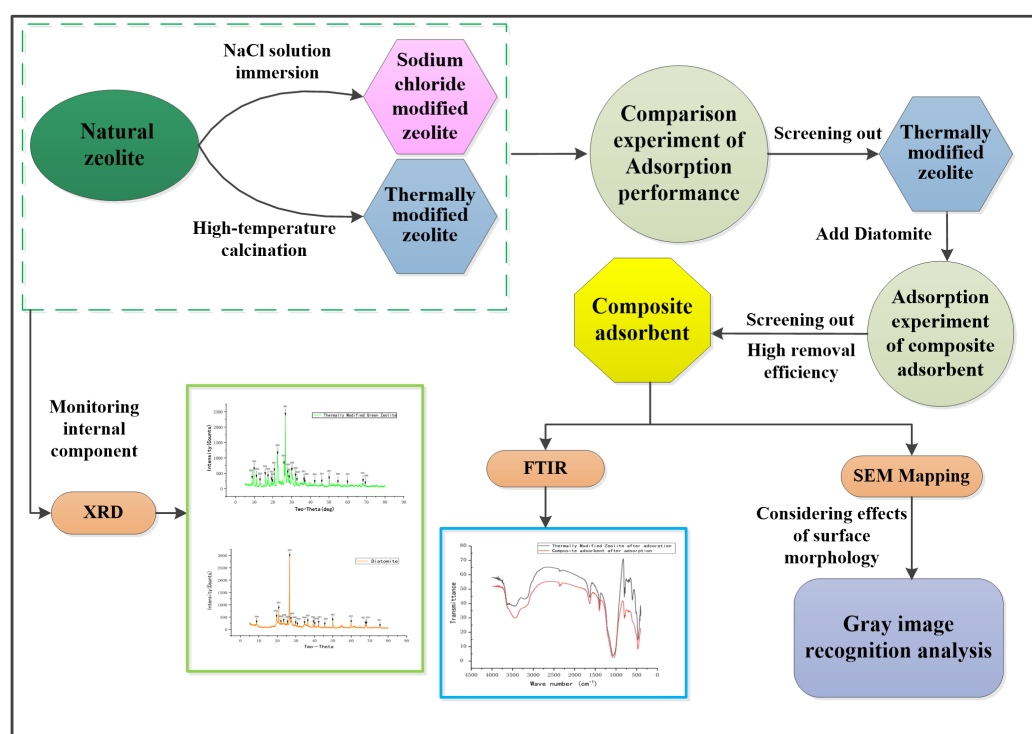


Figure 1. Research framework.

2. Materials and Methods

2.1. Preparation of Composite Adsorbent

The composite adsorbent with improved physical and chemical properties was prepared as follows: First, the proper amount of distilled water was used to rinse green zeolite with impurities repeatedly. Then, the adsorbent was placed in the oven at 105 °C to dry. After drying, the green zeolite was placed in a grinder and over a 200-mesh sieve to crush for 30 s. Then, green zeolite powder with particle sizes less than 0.075 mm was collected and stored in a clean beaker. Similarly, large particles of diatomite, from which impurities were removed, were placed in a large grinder and ground for 30 s through a 200-mesh sieve. Then, diatomite powder with particle sizes less than 0.075 mm was obtained, which was stored in a clean beaker for further use. Next, the pre-treated green zeolite powder in the crucible was weighed and placed in a muffle furnace with temperature adjusted and

maintained at 350 °C. After 3 h, the calcined green zeolite powder was cooled to 25 °C to obtain thermally modified green zeolite and stored in a clean beaker for use. Third, a certain amount of sodium chloride solution with a concentration of 0.4 mol/L was prepared, then weighed green zeolite powder was mixed with this solution at a 1:50 ratio in a centrifuge at a speed of 50 rpm for 3 h. Next, the modified zeolite was removed and rinsed with distilled water repeatedly to remove excess Na⁺ and Cl⁻. Then it was placed in an oven at a temperature of 105 °C. After drying, the zeolite was stored in a clean beaker for further use. Then, through the screening experiment of the adsorbent, thermally modified zeolite was mixed with different ratios of 0.075 mm pre-treated diatomite powder. Finally, the composite adsorbent material was obtained. Figure 2 displays the features of natural green zeolite powder, sodium chloride modified green zeolite powder, thermally modified green zeolite powder and composite adsorbent powder.

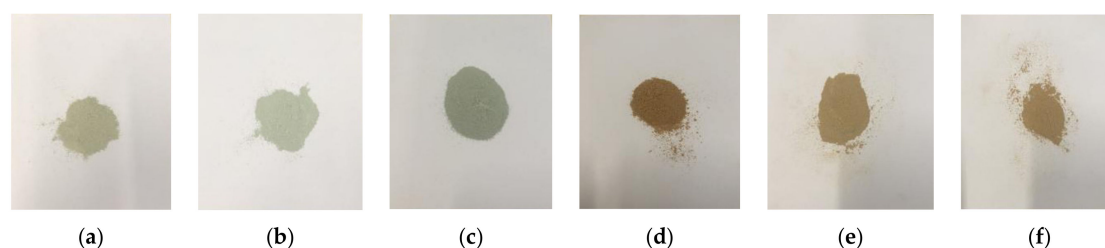


Figure 2. Materials: (a) thermally modified zeolite (TMZ), (b) sodium chloride modified zeolite (SCMZ); (c) natural zeolite (NZ), (d) diatomite (D), (e) composite adsorbent (TMZ/D = 3:2), (f) composite adsorbent (TMZ/D = 2:3).

2.2. Adsorption Experiments

2.2.1. Experimental Design of Nitrogen Adsorption Kinetics

To study the effects of different parameters on adsorption process (e.g., time, initial solution concentration, amount of adsorption), adsorption kinetics experiments of nitrogen were carried out by adding 0.5 g of natural, sodium chloride modified, or thermally modified green zeolite powder and placing it into 250 mL conical flasks containing 50 mL NH₄Cl solution at 25 °C. The concentration of NH₄Cl in the solution was 50 mg/L. The solution pH was adjusted to 7.0 ± 0.1, and the desired pH value of the working solutions was controlled by 0.1 mol/L HCl/NaOH solution, then shaken at 200 rpm in a constant temperature shaker. The above suspensions were withdrawn at 40, 60, 120, 240, 480, 960, and 1440 min, while the supernatant solutions were pipetted and separated by filtration through a 0.45 µm pore size membrane for determination of the remaining NH₄⁺-N concentrations.

2.2.2. Experimental Design of Nitrogen Adsorption Isotherms

The experiments for measuring the adsorption isotherms of nitrogen were conducted in 250 mL conical flasks containing 50 mL of NH₄Cl solution and 2 g of adsorbent: natural, NaCl modified or thermally modified green zeolite powder. The concentration of NH₄Cl solution was set to 5, 10, 20, 30, 40, 60, 80, and 100 mg/L, with the pH adjusted to 7.0 ± 0.1. The flasks were shaken at 200 rpm in a shaker at 25 °C for 3 h. Next, the supernatant solutions were pipetted and separated by filtration through a 0.45 µm pore size membrane for determination of the remaining NH₄⁺-N concentrations.

2.2.3. Experimental Design of Phosphorus Adsorption Kinetics

The adsorption kinetics experiments of phosphorus were carried out by adding 0.5 g of diatomite powder into conical flasks containing 50 mL KH₂PO₄ solution at 25 °C. The concentration of KH₂PO₄ in solution was 5 mg/L. The solution pH was adjusted to 7.0 ± 0.1, and then it was shaken at 200 rpm in a constant temperature shaker. The above suspensions were withdrawn at 40, 60, 120, 240,

480, 960, and 1440 min, while the supernatant solutions were pipetted to determine the remaining phosphorus concentrations.

2.2.4. Experimental Design of Phosphorus Adsorption Isotherms

The experiments for measuring the adsorption isotherms of phosphorus were performed in 250 mL conical flasks containing 50 mL of KH_2PO_4 solution and 0.5 g of diatomite powder. The concentration of KH_2PO_4 solution was set to 5, 10, 20, 30, 40, 60, 80, and 100 mg/L, with the pH adjusted to 7.0 ± 0.1 . The flasks were shaken at 200 rpm in a shaker at 25°C for 3 h. Next, the supernatant solutions were pipetted and separated by filtration through a $0.45\ \mu\text{m}$ pore size membrane for determination of the remaining phosphorus concentrations.

2.2.5. Experimental Design of Composite Adsorbent Experiment

The composite adsorbent experiment examined the combined modified zeolite and diatomite for the purpose of simultaneously adsorbing nitrogen and phosphorus in drainage ditches on farmland. The experimental design process involved mixing the modified zeolite and diatomaceous earth adsorbents in 5 ratios of 1:1, 1:2, 2:1, 3:2, and 2:3. Simultaneous nitrogen and phosphorus removal experiments were conducted to obtain the best composite adsorbent with the same effect of simultaneous nitrogen and phosphorus removal. In accordance with these 5 proportions, the thermally modified zeolite and diatomaceous earth were mixed uniformly, and 5 composite adsorbents were obtained. Then, after pre-treatment of each 2 g of composite adsorbent in a 250 mL conical flask, the mass concentration of NH_4Cl and KH_2PO_4 was combined to achieve (in N, P) 50 mg/L and 5 mg/L standard solution of 50 mL with a pH of 7. Then, the composite was placed in a thermostatic oscillator at a temperature of 25°C and rotational speed of 200 rpm in continuous oscillation for 24 h.

The experiment was conducted in triplicate, and the averages of the results were used for data analysis. The relative error of the data was about 5%. The equilibrium adsorption capacity (q_e , mg/g) and adsorption percentage (%) were calculated from the following equations:

$$q_e = \frac{(C_0 - C_e)V}{m} \quad (1)$$

$$\text{Adsorption percentage (\%)} = \frac{(C_0 - C_e)V}{m} \times 100\% \quad (2)$$

where C_0 and C_e are the initial and final equilibrium concentrations (mg/L), respectively, of N or P in solution, V (mL) is the volume of the solution and m (mg) is the mass of the adsorbent.

2.3. Analytical and Characterization Methods

The composite adsorbent, consisting of thermally modified green zeolite and diatomite, was measured by material composition and structure or configuration of an atom or molecule through XRD. The surface morphology of the adsorbent was determined by scanning electron microscopy (SEM, Hitachi S-4800, Tokyo, Japan). The mapping SEM result was analyzed using greyscale image analysis. Compound structure and functional group type were determined by Fourier-transform infrared spectroscopy (FT-IR, Nicolet iS10, MA, USA) images. Phosphate concentration was determined by the molybdenum blue spectrophotometric method, with a spectrophotometer at 700 nm (UV, Shimadzu UV-2550, Kyoto, Japan). Ammonia nitrogen concentration was determined by Nessler's reagent spectrophotometer method, with a spectrophotometer at 420 nm (UV, Shimadzu UV-2550, Kyoto, Japan).

3. Results and Discussion

3.1. X-ray Diffraction Pattern

Figure 3 displays the XRD profiles of natural green zeolite powder, sodium chloride modified green zeolite powder, thermally modified green zeolite powder, and diatomite composite. Though the natural, thermally modified and sodium chloride modified green zeolite have similar diffraction peaks, the composition of the substance changed after calcination and salt modification treatment. The main phase of the zeolite used for the experiment was silicate minerals, and raw material diatomaceous was mainly composed of cristobalite. As opposed to natural zeolite, the analcime in the thermally modified zeolite disappeared. Meanwhile, quartz and heulandite continued to exist, but a new phase appeared, which was muscovite. This may be due to the fact that zeolite is calcined at high temperatures, which accounts for the change in the crystal structure of natural zeolite, and the elements in the zeolite mutually diffused and reacted with analcime and phlogopite to produce a new phase or solid solution. When zeolite is modified with sodium chloride, some metal salt in the zeolite participates in the reaction, the content of sodium in the sodium chloride modified green zeolite increases and the entire substance is negatively charged. Due to the insertion of sodium ions, the atomic radius increased, which could improve the ability to adsorb ammonia nitrogen.

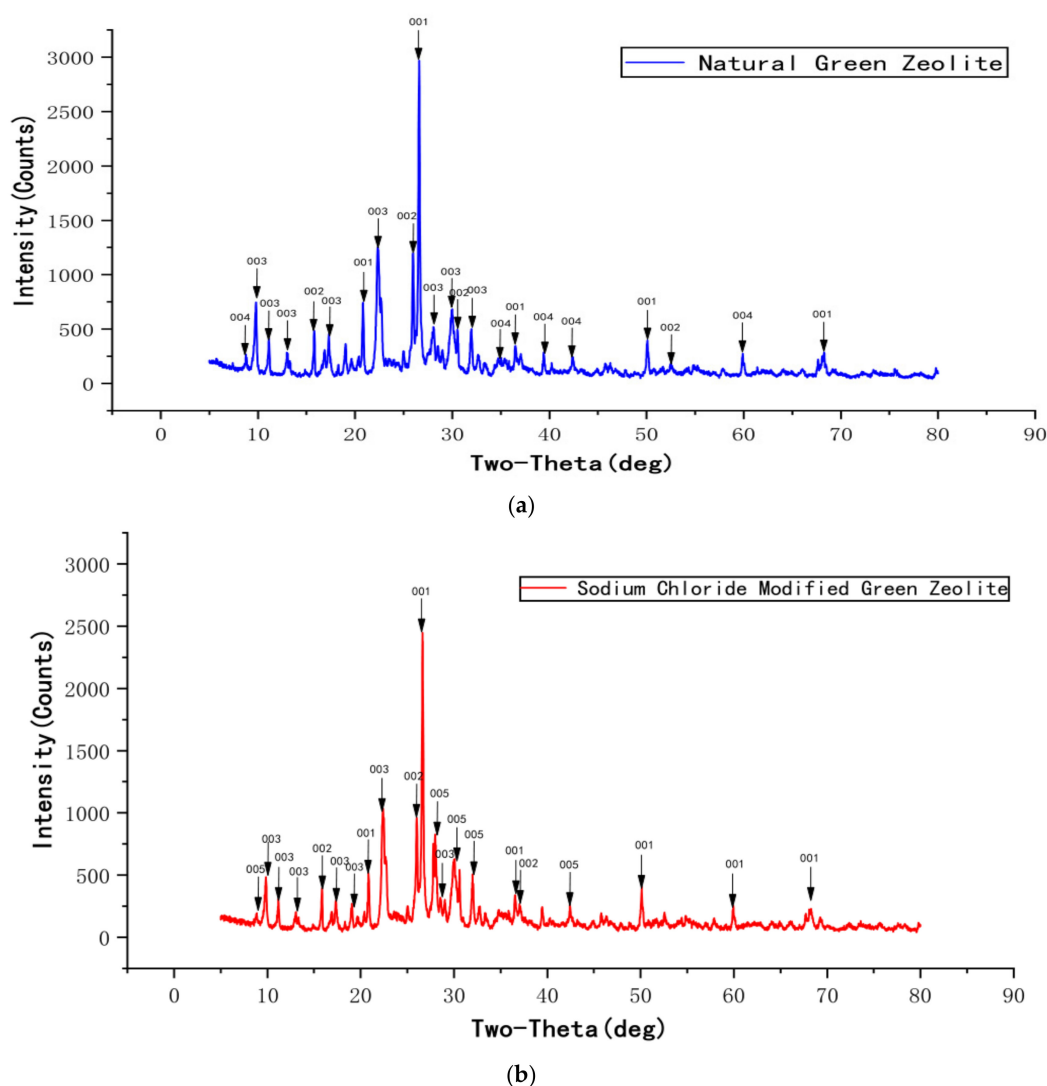


Figure 3. Cont.

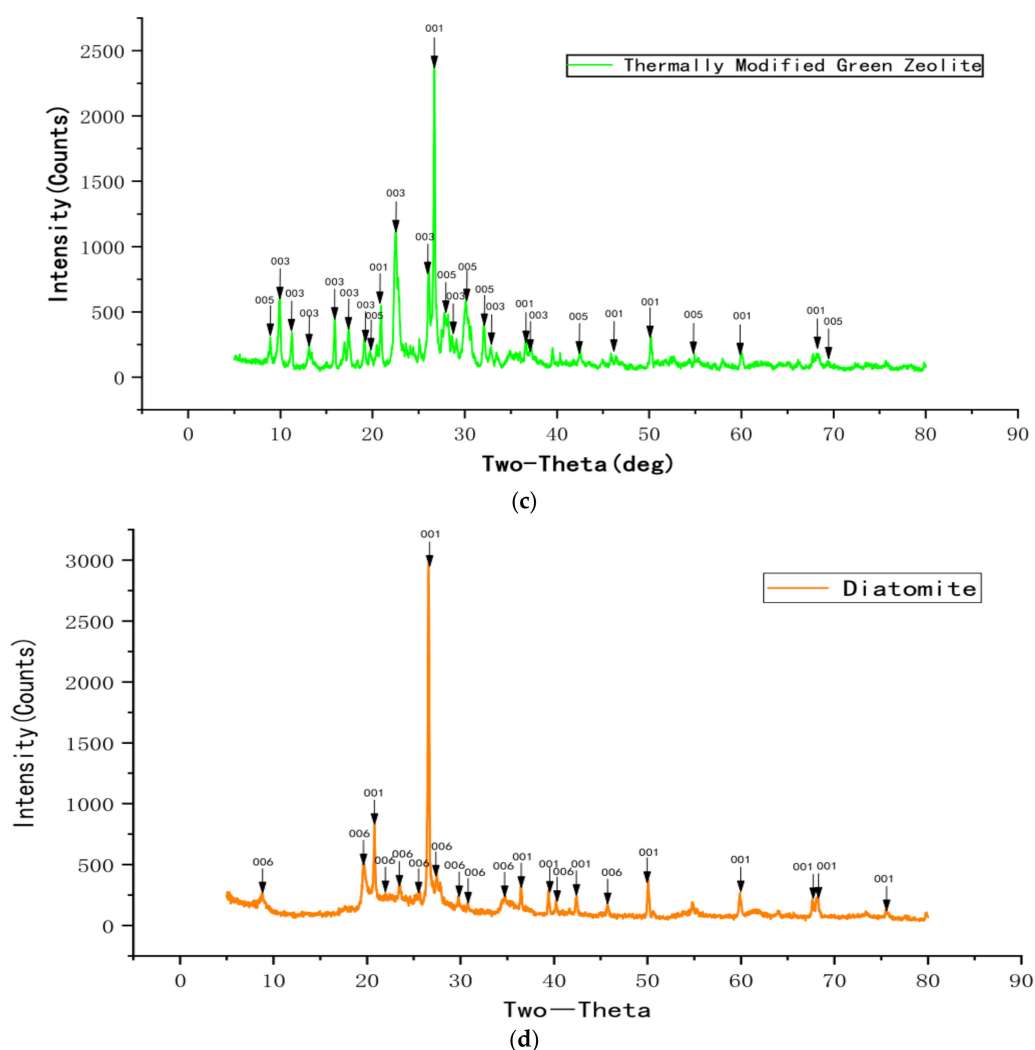


Figure 3. The XRD profiles of natural green zeolite powder (a), sodium chloride modified green zeolite powder (b), thermally modified green zeolite (c), and diatomite composite (d).

3.2. Adsorption Kinetics

3.2.1. Nitrogen Adsorption Kinetics

The nitrogen adsorption kinetics of modified green zeolite at different initial concentrations was investigated by varying the contact time, and the results are presented in Figure 4. It is evident that the adsorption process could be divided into two stages. First is the rapid stage, which occurs before 120 min. In this stage, the three types of zeolites exhibited the phenomenon of rapid adsorption, because the concentration of adsorbate was high at the initial stage of the adsorption process, and there were more available adsorbates for adsorption of the zeolites. Second is a gradually slower stage that occurs after 120 min, in which the adsorption equilibrium is achieved over time, and the adsorption rate was low compared with the initial stage of adsorption. This stage lasted longer, hence the phenomenon could be characterized as “fast adsorption, slow saturation.”

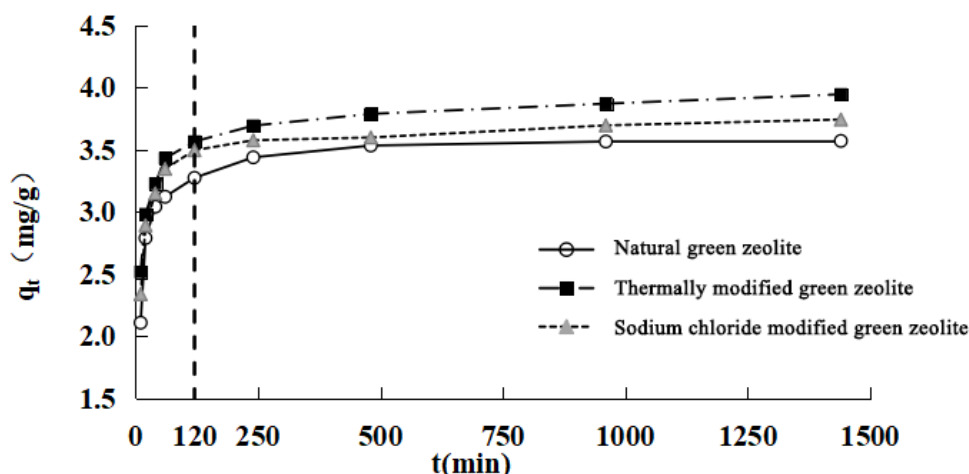


Figure 4. Adsorption kinetics of nitrogen on three kind of zeolites.

For further explanation of the adsorption kinetics, two other kinetic models, pseudo-first-order and pseudo-second-order, were employed. The pseudo-first-order kinetic model is expressed in Equation (3):

$$\ln(q_e - q_t) = \ln q_e - k_1 t \quad (3)$$

where q_e and q_t (mg/g) are the amounts of nitrogen adsorbed on adsorbents at equilibrium and contact time t (min), respectively, and k_1 is the rate constant of the model (min^{-1}). The values of k_1 and q_e can be obtained from the slope and intercept of the linear plots of $\ln(q_e - q_t)$ versus t , as shown in Table 1. The q_e values of natural, NaCl modified and thermally modified green zeolite were calculated (3.40, 3.66, 3.53 mg/g), showing only a small difference compared with the experimental data (3.57, 3.95, 3.74), and the correlation coefficient values (R^2) are 0.8915, 0.8334, 0.7332. These show that the experimental data are not consistent with the pseudo-first-order model. The pseudo-second-order model is represented as Equation (4):

$$\frac{t}{q_t} = \frac{1}{k_2 q_e^2} + \frac{t}{q_e} \quad (4)$$

where k_2 (g/mg·min) is the rate constant for adsorption. As we can see in Table 1, the values of k_2 and q_e can be obtained from the slope and intercept of the plot of t/q_t versus t . It is noticeable that the calculated q_e values for natural, NaCl modified and thermally modified green zeolite of the pseudo-second-order kinetic model (3.59, 3.95, 3.75) are closer to those of the experimental data (3.57, 3.95, 3.74), and the R^2 values (1.0, 0.9999, 0.9998) are higher than those of the pseudo-first-order model, which indicates that the pseudo-second-order kinetic model is more suitable for the adsorption of nitrogen. This indicates that the adsorption of ammonia nitrogen by zeolite is chemical adsorption. This also indicates that the removal of ammonia nitrogen by zeolite is mainly based on ion exchange and supplemented by physical adsorption, consistent with the related studies [19,20].

Table 1. Adsorption kinetic parameters of three kind of zeolites onto nitrogen.

Adsorbent	Pseudo-First-Order Model				Pseudo-Second-Order Model		
	q_t (mg/g)	q_e (mg/g)	k_1 (min^{-1})	R^2	q_e (mg/g)	k_2 (g/mg·min)	R^2
Natural green zeolite	3.57	3.40	0.0807	0.8915	3.59	0.03216	1
Thermally modified green zeolite	3.95	3.66	0.0998	0.7332	3.95	0.02230	0.9998
NaCl modified green zeolite	3.74	3.53	0.0956	0.8334	3.75	0.02867	0.9999

Although the pseudo-first-order and pseudo-second-order kinetic models demonstrated the process of adsorption, the intraparticle diffusion model can perform a deeper study of the process of adsorbing pollutants to determine whether the diffusion mechanism is a limiting step in the adsorption process.

The mathematical equation for the intraparticle diffusion model is:

$$q_t = k_i t^{0.5} \quad (5)$$

where k_i is the intraparticle diffusion rate parameter.

Figure 5 shows that the nitrogen adsorption process of the three types of zeolite can be roughly divided into three stages: first is the rapid external surface adsorption stage; second is the gradual adsorption stage, and intraparticle diffusion is the rate-limiting step of the process in this stage; and third is the final balanced stage. The fitting curve of the second stage clearly does not pass through the origin, which indicates that intraparticle diffusion is not the only rate-limiting step in the adsorption stage, and the rate-limiting step in the gradual adsorption stage includes both liquid film and intraparticle diffusion [21].

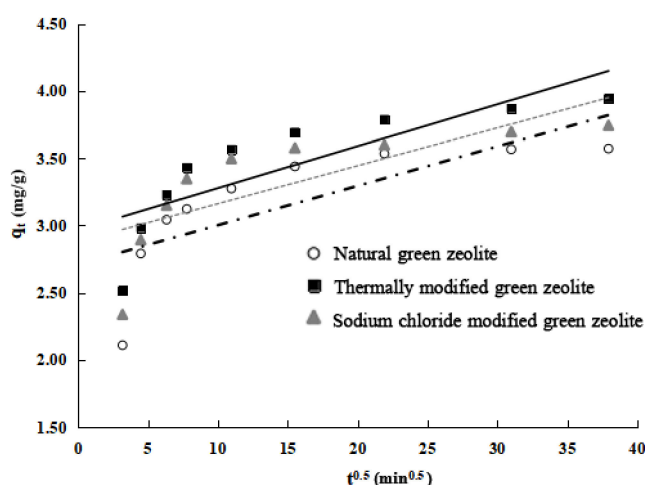


Figure 5. Adsorption curve of three kind of zeolites for q_t onto $t^{0.5}$.

3.2.2. Phosphorus Adsorption Kinetics

The phosphorus adsorption kinetics of diatomite are shown in Figure 6. The figure shows that the unit adsorption capacity of diatomite on phosphate gradually increases with the increased reaction time until an equilibrium is reached. It was shown that the adsorption process could also be divided into two parts: a rapid stage before 240 min, which may be due to the higher concentration of phosphorus during the initial adsorption stage, and the middle and later stages of the process after 240 min, in which the adsorbent gradually reaches saturation and the adsorption rate is lower, which is longer than that in the initial stage. This phenomenon can be characterized as “rapid adsorption, slow saturation.”

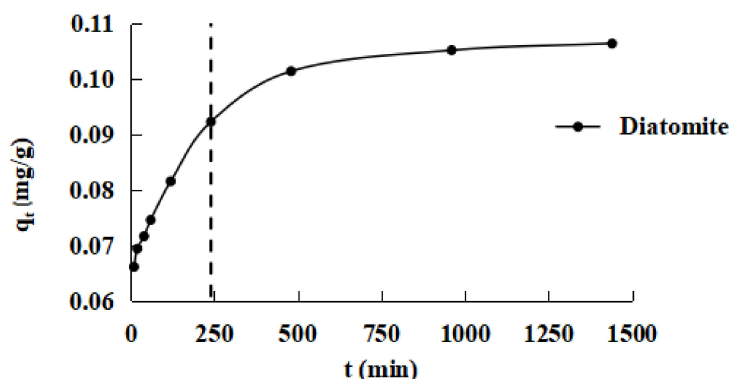


Figure 6. Adsorption kinetics of phosphorus on diatomite.

The pseudo-first-order and a pseudo-second-order kinetic models were used to fit the experimental data. The results are shown in Table 2. The table shows that equilibrium adsorption capacity q_e obtained by the pseudo-second-order kinetic model is closer to the equilibrium adsorption quantity q_t , and R^2 is higher. The pseudo-second-order kinetic model is more suitable for describing the adsorption of diatomite onto phosphorus in water than the pseudo-first-order model. Therefore, the adsorption of ammonia phosphorus by diatomite is chemical adsorption. Chemical adsorption involves valence forces in which the adsorbent and adsorbate share or exchange electrons.

Table 2. Adsorption kinetic parameters of diatomite onto phosphorus.

Adsorbent	Pseudo-First-Order Model			Pseudo-Second-Order Model		
	q_e (mg/g)	k_1 (min ⁻¹)	R^2	q_e (mg/g)	k_2 (g/mg·min)	R^2
Diatomite	0.0909	0.0934	0.2509	0.1078	0.3881	0.9995

The intraparticle diffusion model is used to further study the process of diatomite kinetic adsorption. The experimental results are shown in Figure 7. From the curves of q_t fit to $t^{0.5}$ of diatomite adsorbed phosphorus in Figure 7, the adsorption of phosphorus can be roughly divided into three stages: first is rapid adsorption on the outside surface, second is gradual adsorption, and third is the final balancing. The fitting curve for stage 2 clearly does not pass through the origin, indicating that intraparticle diffusion is not the only rate-limiting step in the gradual adsorption phase of diatomite. Instead, the rate-limiting step includes liquid film and intraparticle diffusion.

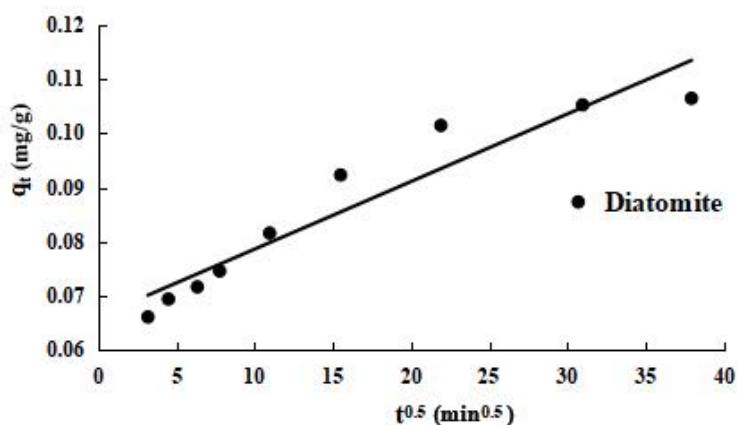


Figure 7. Adsorption curve of diatomite for q_t onto $t^{0.5}$.

3.3. Adsorption Isotherms

3.3.1. Adsorption Isotherms of Three Kind of Zeolites

To clearly understand the surface properties and adsorption behaviour of the three types of zeolite, their adsorption onto nitrogen was investigated by fitting the experimental data with the Langmuir, Freundlich [22], and Dubinin–Radushkevich (D–R) [23] isotherm models. The models are shown in Figure 8a–c. The Langmuir model is based on the assumption that adsorption is localised on a monolayer and there is no interaction between the adsorbed pollutants; the Freundlich isotherm assumes that the process of adsorption occurs on a heterogeneous surface. The three isotherm equations are expressed as follows (Equations (6)–(8)):

$$\text{Langmuir : } \frac{C_e}{q_e} = \frac{C_e}{q_{\max}} + \frac{1}{q_{\max}K_L} \tag{6}$$

$$\text{Freundlich : } \ln q_e = \ln K_F + \frac{1}{n} \ln C_e \tag{7}$$

$$\text{D-R : } \ln q_e = \ln q_0 - K_D \left(RT \ln \left(1 + \frac{1}{C_e} \right) \right)^2 \tag{8}$$

where K_L is the Langmuir isotherm constant, q_e represents the equilibrium adsorption capacity (mg/g), C_e represents the balance mass concentration (mg/L), q_{\max} represents the maximum adsorption capacity of the three types of zeolite on nitrogen, and K_F and n are constants. When the Freundlich isotherm model has a $1/n$ value between 0 and 1, it is classified as preferential adsorption [24]. K_F (mg/g) and $1/n$ are the Freundlich constants related to adsorption capacity and intensity, respectively. K_D is the constant related to adsorption energy (mol^2/kJ^2); $\epsilon = RT \ln(1+1/C_e)$; R is the ideal gas constant, 8.314 J/mol·K; T is absolute temperature (K). When the average adsorption energy E of the adsorbed material is between 8 and 16 kJ/mol, the adsorption process is classified as ion exchange; E is the mean free energy of adsorption, $E = 1/(2K_D)^{0.5}$.

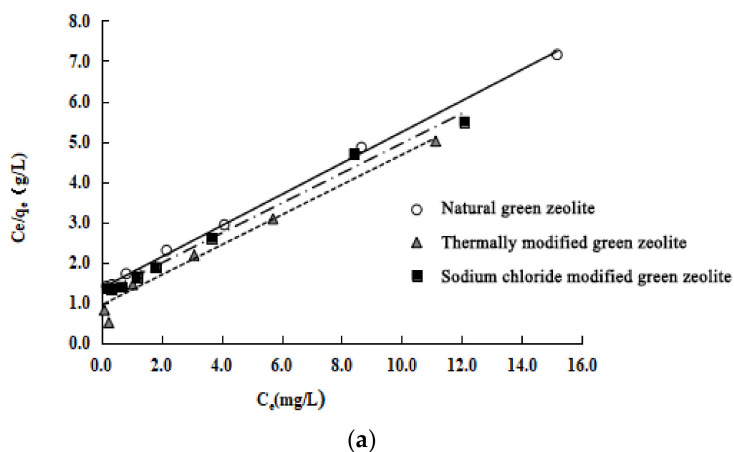
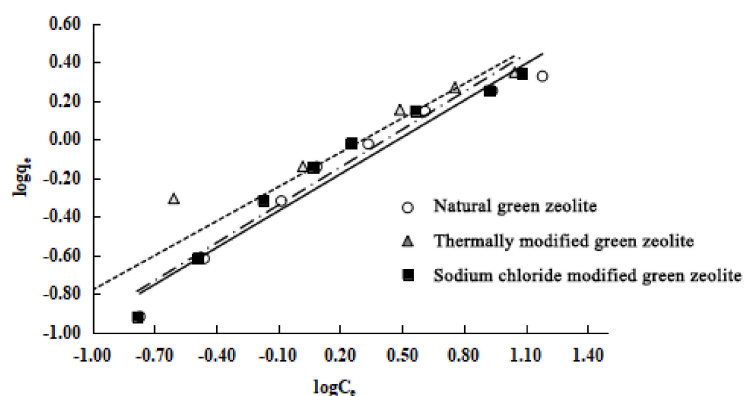
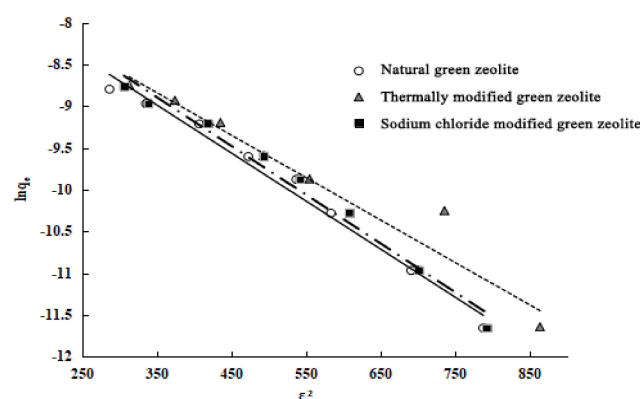


Figure 8. Cont.



(b)



(c)

Figure 8. Isotherm adsorption model of three kind of zeolites onto nitrogen: (a) Langmuir model, (b) Freundlich model and (c) Dubinin–Radushkevich (D–R) model. Solid lines represent natural, dotted lines represent thermally modified and dashed lines represent NaCl modified green zeolite.

The Langmuir, Freundlich, and D–R models are used to study the isothermal adsorption processes of the three types of zeolite. The experiment results, shown in Table 3, are as follows: (1) These three models can describe the isothermal adsorption process of the three kinds of zeolite on nitrogen. (2) The adsorption isotherm is more consistent with the Langmuir model because of its higher correlation coefficients. The Langmuir model assumes that these adsorbents undergo monolayer adsorption. (3) The maximum adsorption capacity of the three types of zeolite is calculated as follows: natural green zeolite, 0.8644 mmol/L; thermally modified green zeolite, 1.0660 mmol/L; and sodium chloride modified green zeolite, 0.9430 mmol/L. (4) The parameter $1/n$ of the adsorption models of natural, thermally modified and NaCl modified zeolite are 0.6512, 0.5920, and 0.6351, respectively, which shows that the nitrogen adsorption process of the zeolites belongs to the preferential adsorption class. (5) The average adsorption energy (E) values of natural, thermally modified, and NaCl modified zeolite calculated by parameter K_D of the D–R model are 9.2851 kJ/mol, 9.9010 kJ/mol, and 9.2851 kJ/mol, ranging from 8 kJ/mol to 16 kJ/mol, indicating that the nitrogen adsorption of the zeolites can be classified as ion exchange.

Table 3. Adsorption isotherm parameters of three kinds of zeolite onto nitrogen.

Adsorbent	Langmuir			Freundlich			D–R		
	q_e (mg/g)	K_L (L/mg)	R^2	K_F	$1/n$	R^2	q_0 (mmol/L)	E (KJ/mol)	R^2
Natural green zeolite	2.5773	0.2870	0.9980	0.5294	0.6512	0.9604	0.9430	9.2851	0.9837
Thermally modified green zeolite	2.6795	0.3991	0.9671	0.6489	0.5920	0.9223	0.8644	9.9010	0.9338
NaCl modified green zeolite	2.6925	0.3007	0.9903	0.4918	0.6351	0.9590	1.0660	9.2851	0.9816

3.3.2. Adsorption Isotherms of Diatomite

The experimental results of investigating the adsorption process of diatomite by the Langmuir, Freundlich, and D–R models [25] are shown in Table 4. From the fitting results, we can find the following: (1) The three models can describe the isothermal adsorption of diatomite onto phosphate. (2) Compared with the Langmuir and Freundlich models, the D–R model can describe this process more completely. (3) The Freundlich model parameter $1/n$ of diatomite is 0.8146, which is between 0 and 1, hence it can be classified as preferential adsorption. (4) The average adsorption energy (E) value of diatomite calculated by parameter K_D of the D–R model was 9.53 kJ/mol, ranging from 8 kJ/mol to 16 kJ/mol, indicating that the phosphate adsorption of diatomite is ion exchange.

Table 4. Adsorption isotherm parameters of three kinds of diatomite onto phosphorus.

Adsorbent	Langmuir			Freundlich			D–R		
	q_e (mg/g)	K_L (L/mg)	R^2	K_F	$1/n$	R^2	q_0 (mmol/L)	E (KJ/mol)	R^2
Diatomite	0.4602	0.9244	0.9709	0.2464	0.8146	0.9950	0.2691	9.5300	0.9990

3.4. Adsorption Experiment of Composite Adsorbent

The adsorption capacity of composite adsorbent on nitrogen and phosphorus was investigated by regulating the proportion of the mix of thermally modified green zeolite and diatomite, presented in Figure 9. As the proportion of thermally modified zeolite in the composite adsorbent is decreased gradually, the ability of the composite adsorbent to adsorb nitrogen in water gradually decreases. Similarly, as the proportion of diatomite accounts for the gradual increase in composite adsorbent, the phosphate adsorption ability of composite adsorbent in water also gradually increases. When the ratio of thermally modified zeolite to diatomite is 2:3, the composite adsorbent exhibits good efficiency to adsorb nitrogen and phosphorus in water, with a removal efficiency of 88.54% and 91.08%, respectively. When the ratio of thermally modified zeolite to diatomite is 3:2, the composite adsorbent removal rate of nitrogen and phosphorus is 92.07% and 84.61%, respectively. According to experimental studies, nitrogen pollution is more serious than phosphorus pollution in farmland drainage. Therefore, we decided to use composite adsorbent with a compound ratio of 3:2 for in-depth study. Up to now, there have been some studies on the removal of nitrogen and phosphorus from water by modified zeolite and diatomite. Stocker et al. [26] investigated the influence of highly concentrated reagents (NaCl, 22.36%; HCl, 20%; NaOH, 32%) on the mineralogy (e.g., structure and mineral chemistry) and NH_4^+ exchange capacity of a natural zeolite (particle size 0.05–0.2 mm). Based on adsorption performance experiments, NaCl–zeolite was shown to be an excellent material to adsorb nitrogen, and the removal rate reached about 65%. Wu et al. [27] proposed a highly efficient adsorbent for low-concentration phosphate removal from aqueous solution made of hydrated lanthanum (La) oxide-modified diatomite composite (La-diatomite). The maximum capacity to remove phosphorus reached 96%. By comparison, it was found that the composite adsorbent in this study had a better adsorption effect on ammonia nitrogen and phosphorus in water.

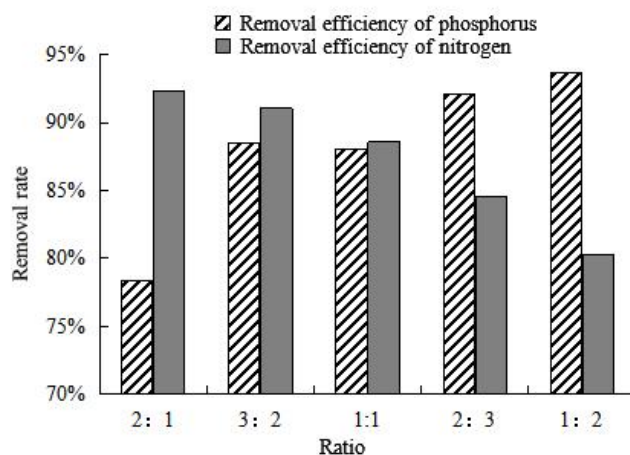
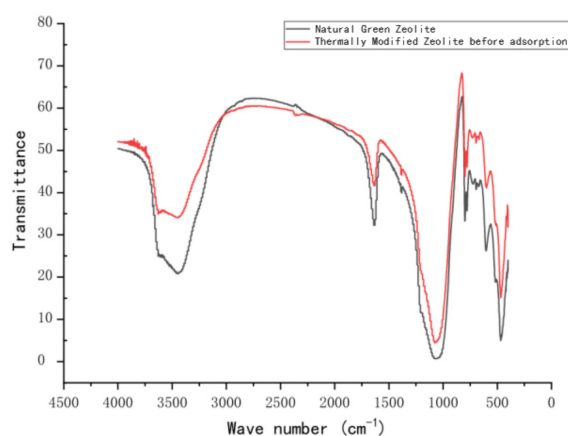


Figure 9. Column chart of adsorption efficiency of different proportions of thermally modified zeolite and diatomite on nitrogen and phosphorus.

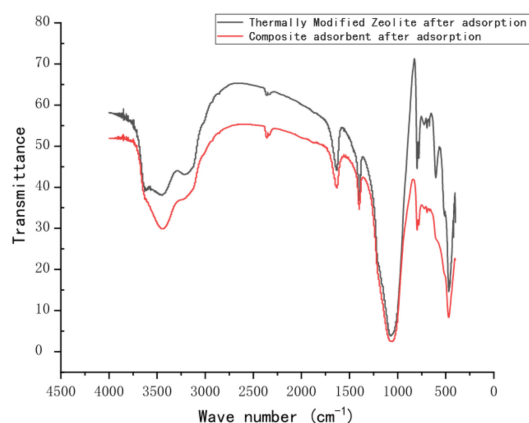
3.5. Fourier Transform Infrared Spectroscopy (FT-IR) Analysis

Fourier-transform infrared spectra were obtained using an FT-IR spectrophotometer (FT-IR, Nicolet iS10, American state of Massachusetts). The FT-IR spectra (Figure 10) displayed variations in functional groups on the surface of the zeolite before and after modification. They also show changes in the nitrogen functional group before and after adsorption. The infrared spectra of natural zeolite and calcined zeolite are shown in Figure 10a. The bending vibration peak appears at 564 cm^{-1} , which was attributed to the vibration adsorption peak of Fe–O. The peak at 1568 cm^{-1} corresponds to the vibration peak of Al–O, and that at 1061 cm^{-1} can be matched with the vibration of the Si–O–Si skeleton. In addition, there is an adsorption peak of bound water at $3000\text{--}3500\text{ cm}^{-1}$, which corresponds to the antisymmetric vibration of the –OH group, and the maximum absorption peaks of zeolite and thermally modified zeolite are located at 3454 cm^{-1} and 3447 cm^{-1} , respectively, mainly due to the difference in the bending vibration of combined water after the thermal modification of zeolite, consistent with previous studies [28,29]. The infrared spectra of calcined green zeolite and composite adsorbent after the respective adsorption (thermally modified green zeolite and diatomite at a ratio of 3:2) are shown in Figure 10b. Surprisingly, the absorption peaks of calcined green zeolite and composite adsorbent are located at 3150 cm^{-1} and 1400 cm^{-1} , respectively, after the respective adsorption, which are N–H group vibration peaks, indicating that ammonia nitrogen was adsorbed into the internal pores of the zeolite molecular sieve.



(a)

Figure 10. Cont.



(b)

Figure 10. FT-IR spectra of (a) natural green and thermally modified zeolite and (b) thermally modified zeolite and composite adsorbent after adsorption.

3.6. SEM Analysis

The surface morphology of the modified zeolite and diatomite is shown in Figure 11. It can be observed that the surface of the zeolite is relatively glossy and smooth. After recombination with a certain proportion of diatomite, the surface of composite adsorbent is newly covered with protrusions. Figure 11a shows a scanning electron micrograph of thermally modified green zeolite, which does not have a regular surface morphology, and there is little agglomeration. Figure 11b shows the SEM image of diatomite, with a microstructure composed of sheets of diatomaceous earth, irregularly arranged and partially overlapping. Figure 11c,d shows SEM images of thermally modified green zeolite and diatomite at the ratio of 3:2 and 2:3, respectively. Compared with the morphology of zeolite and diatomite, the structure of compound adsorbent is loose, forming a number of coral-like surface structures. Accompanied by a network of microporous structures, compound adsorbent is widely distributed, with a greatly increased specific surface area to improve the ability to adsorb ammonia nitrogen and phosphorus. Many studies have been done on Brunauer–Emmett–Teller (BET) [30]. The specific surface area of NaCl modified and thermally modified green zeolite was improved after modification to some extent. Our study is more focused on the surface adsorption mechanism of nitrogen and phosphorus, and the effect of BET was not considered.

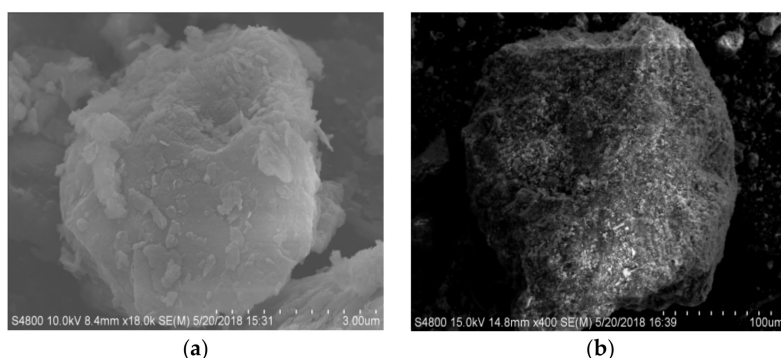


Figure 11. Cont.

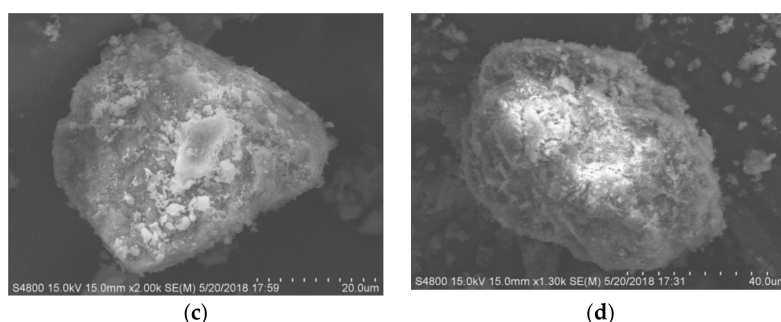


Figure 11. SEM images of (a) zeolite, (b) diatomite, and (c,d) thermally modified green zeolite and diatomite at a ratio of 3:2 and 2:3, respectively.

3.7. Greyscale Analysis

The SEM image of the adsorbent is a greyscale image, which includes 256 grey levels and a greyscale range of 0–255. The grayscale image is composed of grid-like pixels, and the brightness of each pixel corresponds to a grey value. The differences in grey values reflect the different micro-morphology of the particle surface. The higher the resolution of the scanning electron microscope, the more the sediment is the same. The more SEM image pixels the particles get, the clearer the image and the richer the image information.

The S-4800 x-ray energy spectrometer (SEM, Hitachi S-4800, Tokyo, Japan) was used to map the surface of composite adsorbent with a ratio of thermally modified zeolite to diatomite of 3:2. The mapping scan of the adsorbed elemental N and P is shown in Figure 12. According to the image display, the bright green and blue spots in the figure represent the adsorption of nitrogen and phosphorus on the surface of a composite adsorbent single particle with a ratio of thermally modified zeolite to diatomite of 3:2. The black area represents zero adsorption of nitrogen and phosphorus.

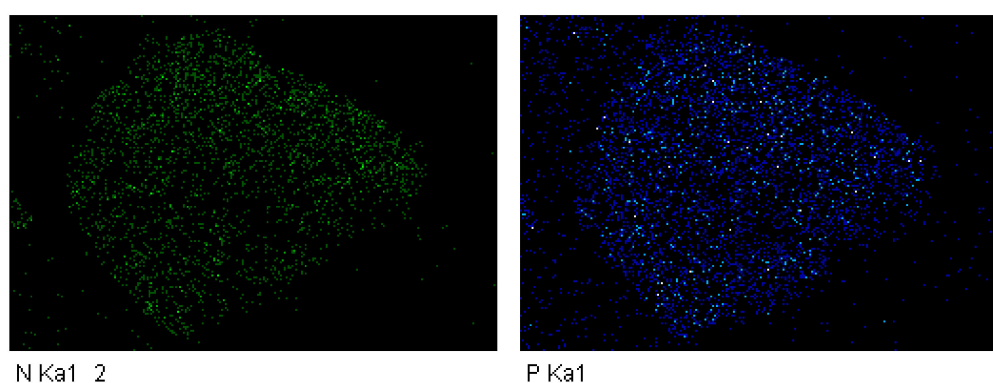


Figure 12. Mapping scan of adsorbed N and P elements of composite adsorbent.

Images of adsorbent particles can be obtained by scanning electron microscopy, reflecting the microscopic characteristics of the surface of the sediment particles. The derivative of the surface greyscale can approximately reflect the gradient reaction of particle surface height distribution.

The first-order gradient reaction on the surface of the adsorbent reflects its roughness. The greater the difference in the gradient, the more undulating the surface of the adsorbent. The second-order gradient reflects the sags and crests on the surface, reflecting the proportion of peaks and valleys. For a continuous function, the first derivative of $f(x,y)$ can be expressed as a vector whose expression is as follows:

$$\nabla f(x, y) = [G_x G_y]^T = \left[\frac{\partial f}{\partial x} \frac{\partial f}{\partial y} \right]^T \quad (9)$$

The vector magnitude and direction angle are:

$$\text{mag}(\nabla f) = [G_x^2 + G_y^2]^{1/2} \quad (10)$$

Generally, to calculate the pixel points of each grey image according to the partial derivative of the above formula, a small area template approximation is used for G_x and G_y . The two templates are combined to form a gradient operator. The operator performs a convolution integral calculation to convolute the image with the horizontal template G_x to obtain a horizontal gradient image. This has a strong effect on the vertical edge and is convolved with the vertical template G_y to obtain a vertical gradient map, which has a strong effect on the horizontal edge. The Sobel operator gradient template performs better and Sobel operator gradient template (a) and (b) are as follows:

-1	0	+1		+1	+2	+1
-2	0	+2		0	0	0
-1	0	+1		-1	-2	-1
(a)			(b)			

An image of the particle greyscale and amplitude characteristics of the composite adsorbent particles is shown in Figure 13. A gradient image of the original greyscale image in the x - and y -directions can be obtained by the Sobel operator. The grey gradient feature map can truly reflect the fluctuation of the surface height of the particle surface; the more surface protrusions, the brighter the display and the larger the gradient value. In addition, the larger the surface depression, the smaller the gradient value. The gradient features in the x - and y -directions are more demonstrable, as shown in Figure 13.

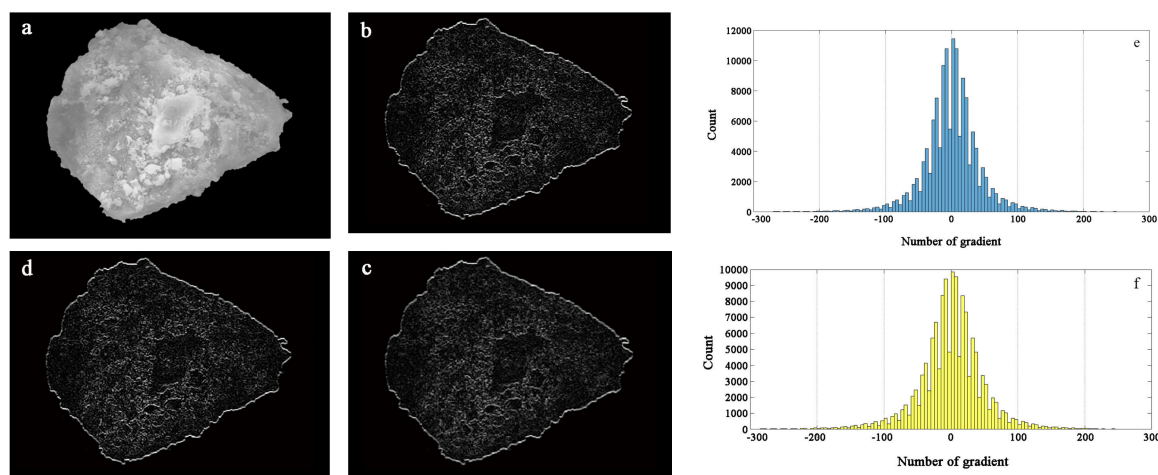


Figure 13. Particle greyscale and amplitude characteristics: (a) original greyscale image, (b) horizontal gradient of greyscale, (c) vertical gradient of greyscale, (d) first-order gradient of greyscale, (e) horizontal gradient feature, (f) vertical gradient feature.

The gradient statistical histogram in the x - and y -directions reflects the range of the gradient distribution in each direction. The two directions are basically similar, and the distribution is primarily in the range of -150 to 150 . The distribution is relatively scattered, and the numerical statistics are shown in Figure 13. It can be seen that the grey point gradient is more prominent in the range of -50 to 50 , indicating that the surface of zeolite particles is irregularly changed, the relief becomes more uneven, and the surface morphology changes are significant.

Laplacian transform is commonly used as a second-order derivative operator. For continuous function $f(x,y)$, the Laplacian operator can be used to calculate the second-order derivative of the SEM

image of the adsorbent. The second derivative histogram can be calculated by MATLAB (MathWorks, Natick, MA, USA). The Laplacian value is, for most pixels, near zero. Combined with the first derivative histogram, the degree of unevenness of the particle surface can be seen. The first-order derivative histogram can be used to detect the unevenness of the particle surface, indicating the roughness and complex appearance of the particle. SEM mapping, greyscale image recognition, and gradient recognition were used to compare the distribution of contaminants and the morphology of the adsorbent surface. The images of the second-order derivative characteristic map and the grey histogram are shown in Figure 14.

The Laplacian operator is as follows:

$$\nabla^2 f = \frac{\partial^2 f}{\partial x^2} + \frac{\partial^2 f}{\partial y^2} \tag{11}$$

The Laplacian operator gradient template (a) and (b) are as follows:

-1	-1	-1	0	-1	0
-1	+8	-1	-1	+4	-1
-1	-1	-1	0	-1	0

(a)
(b)

The uneven data of the histogram show large surface roughness of the composite adsorbent. Combined with second-order gradient histogram, it can be seen that the number of Laplace values is greater than zero, and the phase is near zero. At most, the surfaces of the particles are uneven and the shapes are complicated. SEM mapping and greyscale gradient identification are used to compare and analyze the distribution of pollutants and the morphological contrast of the adsorbent surface. It can be seen that the larger the surface of the gradient, the more uneven it is, the more nitrogen and phosphorus sites are adsorbed on the surface, and the more nitrogen and phosphorus are adsorbed.

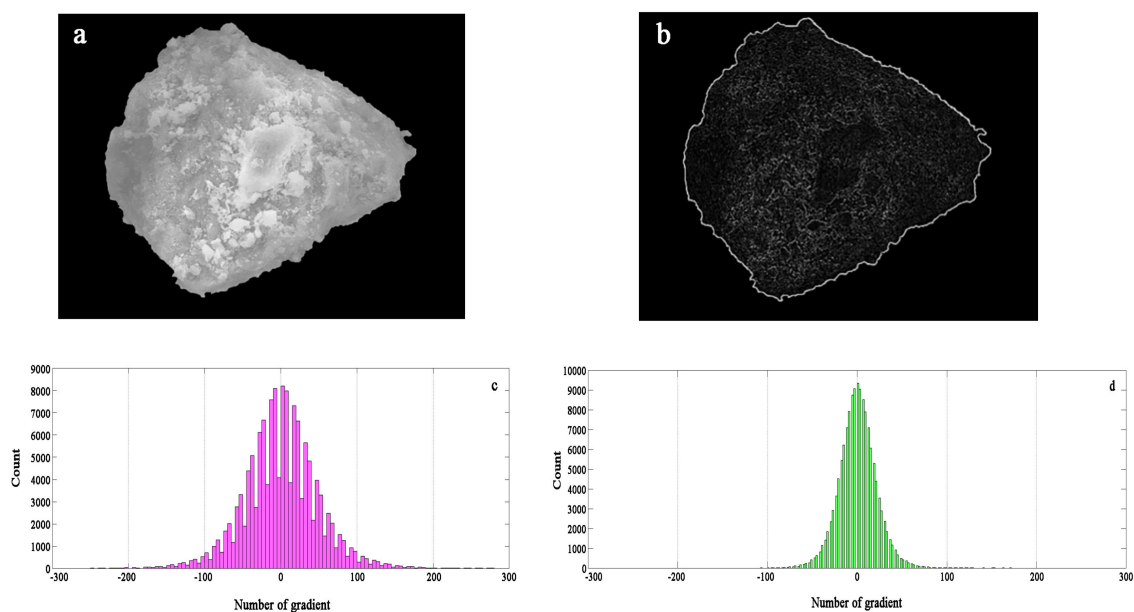


Figure 14. Gradient feature of Laplacian operator: (a) original gray scale image, (b) vertical gradient feature, (c) second-order gradient of Laplacian operator under template a, (d) second-order gradient of Laplacian operator under template b.

4. Conclusions

In this study, based on an experimental examination of adsorption properties, a composite adsorbent with high removal of nitrogen and phosphorus was prepared and tested. SEM mapping combined with greyscale and gradient recognition was used to study the distribution of pollutants and the surface morphology of adsorbents. The composite adsorbents were investigated not only from the perspective of the internal chemical mechanism but also, more importantly, in terms of the surface adsorption morphology and distribution of pollutants. Specifically, the following four conclusions are made, in detail:

(1) Adsorption-modified kinetics and isothermal adsorption experiments were used to screen out thermally modified zeolite for higher removal of nitrogen. It was demonstrated that there are three stages of nitrogen and phosphorus adsorption by zeolite and diatomite: rapid external surface adsorption, gradual adsorption, and final balance. The gradual adsorption stage includes not only intraparticle diffusion, but also liquid film diffusion. The adsorption of nitrogen by zeolite and the adsorption of phosphorus by diatomite can be classified as ion exchange.

(2) Through the relevant experiments, thermally modified zeolite and diatomite were selected to prepare the composite adsorbent. When the proportion of thermally modified zeolite and diatomite was 3:2, the efficiency of removing nitrogen and phosphorus in the water was higher than that of the other structures, reaching 91.08% and 88.54%, respectively.

(3) Modification of the adsorbent and the adsorption process was confirmed by characterization techniques (XRD, SEM, and FT-IR), which were used to study the internal elemental composition, surface morphology, and chemical bonds before and after modification and adsorption. The processes of modification and adsorption have a certain influence on the elemental composition and structure of the adsorbent itself.

(4) In terms of the composite adsorbent obtained by screening, SEM mapping, grey image recognition, and gradient recognition were used to determine the distribution of pollutants and the morphology of the adsorbent surface. There is a particular relationship between the nature of the distribution and the amount of adsorption. It can be seen that the larger the surface of the gradient, the more uneven it is, and the more nitrogen and phosphorus are adsorbed.

In summary, this method has significant value for determining the adsorption mechanism of adsorbents and the overall adsorption process, particularly in practical terms. We will prepare powdered composite adsorbent as ecological concrete blocks and take them to farmland drainage ditches, ecological ponds, and other ecosystems, which will be of considerable help in agricultural non-point-source pollution control. Future work will address high-efficiency nitrogen and phosphorus adsorbents, the overall change in adsorption, the distribution of elemental and internal adsorption of nitrogen and phosphorus, and elemental composition changes. This study provides technical guidance for the preparation of adsorbents to facilitate highly efficient nitrogen and phosphorus removal.

Author Contributions: B.Z. and S.L. conceived, designed and wrote the paper; X.W. provided the help of program implementation and funds; Y.L., Y.A. and X.Z. revised the manuscript.

Funding: This research was funded by the Water Pollution Control and Management of National Science and Technology Major Projects in China (2017ZX07204-003) and the Science Fund for Creative Research Groups of the National Natural Science Foundation of China Grant No. 51621092.

Conflicts of Interest: The authors declare no conflict of interest.

References

1. Rittmann, B.E.; Mayer, B.; Westerhoff, P.; Edwards, M. Capturing the lost phosphorus. *Chemosphere* **2011**, *84*, 846–853. [[CrossRef](#)] [[PubMed](#)]
2. Fernández-Calviño, D.; Bermúdez-Couso, A.; Arias-Estévez, M.; Nóvoa-Muñoz, J.C.; Fernández-Sanjurjo, M.J.; Álvarez-Rodríguez, E.; Núñez-Delgado, A. Competitive adsorption/desorption of tetracycline, oxytetracycline and chlortetracycline on two acid soils: Stirred flow chamber experiments. *Chemosphere* **2015**, *134*, 361–366. [[CrossRef](#)] [[PubMed](#)]
3. Chen, W.-R.; Huang, C.-H. Adsorption and transformation of tetracycline antibiotics with aluminum oxide. *Chemosphere* **2010**, *79*, 779–785. [[CrossRef](#)]
4. Huang, G.; Liu, F.; Yang, Y.; Deng, W.; Li, S.; Huang, Y.; Kong, X. Removal of ammonium-nitrogen from groundwater using a fully passive permeable reactive barrier with oxygen-releasing compound and clinoptilolite. *J. Environ. Manag.* **2015**, *154*, 1–7. [[CrossRef](#)] [[PubMed](#)]
5. He, Y.; Lin, H.; Dong, Y.; Wang, L. Preferable adsorption of phosphate using lanthanum-incorporated porous zeolite: Characteristics and mechanism. *Appl. Surf. Sci.* **2017**, *426*, 995–1004. [[CrossRef](#)]
6. Wu, K.; Li, Y.; Liu, T.; Zhang, N.; Wang, M.; Yang, S.; Wang, W.; Jin, P. Evaluation of the adsorption of ammonium-nitrogen and phosphate on a granular composite adsorbent derived from zeolite. *Environ. Sci. Pollut. Res.* **2019**, *26*, 17632–17643. [[CrossRef](#)] [[PubMed](#)]
7. Mahardika, D.; Park, H.; Choo, K. Chemosphere Ferrihydrite-impregnated granular activated carbon (FH@GAC) for efficient phosphorus removal from wastewater secondary effluent. *Chemosphere* **2018**, *207*, 527–533. [[CrossRef](#)] [[PubMed](#)]
8. Goscińska, J.; Ptaszowska-koniarz, M.; Frankowski, M.; Franus, M.; Panek, R.; Franus, W. Removal of phosphate from water by lanthanum-modified zeolites obtained from fly ash. *J. Colloid Interface Sci.* **2018**, *513*, 72–81. [[CrossRef](#)] [[PubMed](#)]
9. Da Silva, L.C.R.; Zadinelo, I.V.; Moesch, A.; dos Santos, L.D.; Alves, H.J.; Colpini, L.M.S. Influence of the chemical composition of smectites on the removal of ammonium ions from aquaculture effluents. *J. Mater. Sci.* **2014**, *50*, 1865–1875.
10. Zhao, Y.; Geng, J.; Wang, X.; Gu, X.; Gao, S. Tetracycline adsorption on kaolinite: pH, metal cations and humic acid effects. *Ecotoxicology* **2011**, *20*, 1141–1147. [[CrossRef](#)] [[PubMed](#)]
11. Magdy, A.; Fouad, Y.; Abdel-Aziz, M.H.; Konsowa, A. Synthesis and characterization of Fe₃O₄/kaolin magnetic nanocomposite and its application in wastewater treatment. *J. Ind. Eng. Chem.* **2017**, *56*, 299–311. [[CrossRef](#)]
12. Li, Z.; Qi, M.; Tu, C.; Wang, W.; Chen, J.; Wang, A.-J. Highly efficient removal of chlorotetracycline from aqueous solution using graphene oxide/TiO₂ composite: Properties and mechanism. *Appl. Surf. Sci.* **2017**, *425*, 765–775. [[CrossRef](#)]
13. Skubiszewska-Zięba, J.; Charnas, B.; Leboda, R.; Gun'ko, V. Carbon-mineral adsorbents with a diatomaceous earth/perlite matrix modified by carbon deposits. *Microporous Mesoporous Mater.* **2012**, *156*, 209–216. [[CrossRef](#)]
14. Widiastuti, N.; Wu, H.; Ang, H.M.; Zhang, D. Removal of ammonium from greywater using natural zeolite. *Desalination* **2011**, *277*, 15–23. [[CrossRef](#)]
15. He, J.; Li, Y.; Wang, C.; Zhang, K.; Lin, D.; Kong, L.; Liu, J. Rapid adsorption of Pb, Cu and Cd from aqueous solutions by β -cyclodextrin polymers. *Appl. Surf. Sci.* **2017**, *426*, 29–39. [[CrossRef](#)]
16. Liu, Q.; Li, F.; Lu, H.; Li, M.; Liu, J.; Zhang, S.; Sun, Q.; Xiong, L. Enhanced dispersion stability and heavy metal ion adsorption capability of oxidized starch nanoparticles. *Food Chem.* **2017**, *242*, 256–263. [[CrossRef](#)] [[PubMed](#)]
17. Yang, F.; Sun, L.; Xie, W.; Jiang, Q.; Gao, Y.; Zhang, W.; Zhang, Y. Nitrogen-functionalization biochars derived from wheat straws via molten salt synthesis: An efficient adsorbent for atrazine removal. *Sci. Total. Environ.* **2017**, *607*, 1391–1399. [[CrossRef](#)]
18. Fang, H.; Chen, M.; Chen, Z.; Zhao, H.; He, G. Simulation of sediment particle surface morphology and element distribution by the concept of mathematical sand. *HydroResearch* **2014**, *8*, 186–193. [[CrossRef](#)]
19. Zhang, M.; Zhang, H.; Xu, D.; Han, L.; Niu, D.; Zhang, L.; Wu, W.; Tian, B. Ammonium removal from aqueous solution by zeolites synthesized from low-calcium and high-calcium fly ashes. *Desalination* **2011**, *277*, 46–53. [[CrossRef](#)]

20. Juan, R.; Hernandez, S.; Andrés, J.M.; Ruiz, C. Ion exchange uptake of ammonium in wastewater from a Sewage Treatment Plant by zeolitic materials from fly ash. *J. Hazard. Mater.* **2009**, *161*, 781–786. [[CrossRef](#)]
21. Mezenner, N.Y.; Bensmaili, A. Kinetics and thermodynamic study of phosphate adsorption on iron hydroxide-eggshell waste. *Chem. Eng. J.* **2009**, *147*, 87–96. [[CrossRef](#)]
22. Malekian, R.; Abedi-Koupai, J.; Eslamian, S.S.; Mousavi, S.F.; Abbaspour, K.C.; Afyuni, M. Ion-exchange process for ammonium removal and release using natural Iranian zeolite. *Appl. Clay Sci.* **2011**, *51*, 323–329. [[CrossRef](#)]
23. Ngah, W.W.; Fatinathan, S. Adsorption characterization of Pb(II) and Cu(II) ions onto chitosan-tripolyphosphate beads: Kinetic, equilibrium and thermodynamic studies. *J. Environ. Manag.* **2010**, *91*, 958–969. [[CrossRef](#)] [[PubMed](#)]
24. Saltali, K.; Sari, A.; Aydın, M. Removal of ammonium ion from aqueous solution by natural Turkish (Yıldızeli) zeolite for environmental quality. *J. Hazard. Mater.* **2006**, *141*, 258–263. [[CrossRef](#)] [[PubMed](#)]
25. Hsieh, C.-T.; Teng, H. Liquid-Phase Adsorption of Phenol onto Activated Carbons Prepared with Different Activation Levels. *J. Colloid Interface Sci.* **2000**, *230*, 171–175. [[CrossRef](#)]
26. Stocker, K.; Ellersdorfer, M.; Lechleitner, A.; Lubensky, J.; Raith, J.G. Impact of concentrated acid, base and salt pretreatments on the characteristics of natural clinoptilolite and its ammonium uptake from model solution and real effluents. *Microporous Mesoporous Mater.* **2019**, *288*, 109553. [[CrossRef](#)]
27. Wu, Y.; Li, X.; Yang, Q.; Wang, D.; Xu, Q.; Yao, F.; Chen, F.; Tao, Z.; Huang, X. Hydrated lanthanum oxide-modified diatomite as highly efficient adsorbent for low-concentration phosphate removal from secondary effluents. *J. Environ. Manag.* **2019**, *231*, 370–379. [[CrossRef](#)]
28. Wang, J.; Huang, Y.; Pan, Y.; Mi, J. Microporous and Mesoporous Materials Hydrothermal synthesis of high purity zeolite A from natural kaolin without calcination. *Microporous Mesoporous Mater.* **2014**, *199*, 50–56. [[CrossRef](#)]
29. Round, C.I.; Hill, S.J.; Latham, K.; Williams, C.D. The crystal morphology of zeolite A. The effects of the source of the reagents. *Microporous Mater.* **1997**, *11*, 213–225. [[CrossRef](#)]
30. Sun, Q.; Hu, X.; Zheng, S.; Sun, Z.; Liu, S.; Li, H. Influence of calcination temperature on the structural, adsorption and photocatalytic properties of TiO₂ nanoparticles supported on natural zeolite. *Powder Technol.* **2015**, *274*, 88–97. [[CrossRef](#)]



© 2019 by the authors. Licensee MDPI, Basel, Switzerland. This article is an open access article distributed under the terms and conditions of the Creative Commons Attribution (CC BY) license (<http://creativecommons.org/licenses/by/4.0/>).